Fossil coccolith morphological attributes as a new proxy for deep ocean carbonate chemistry

Authors: Amanda Gerotto[1,3]*, Hongrui Zhang[2]*, Renata Hanae Nagai[3], Heather M. Stoll[2], Rubens César Lopes Figueira[1], Chuanlian Liu[4], Iván Hernández-Almeida[2]

[1]Oceanographic Institute, University of São Paulo, São Paulo, Brazil; [2]Geological Institute, ETH Zurich, Zurich, Switzerland; [3]Center for Marine Studies, Federal University of Paraná, Pontal do Paraná, Brazil; [4]State Key Laboratory of Marine Geology, Tongji University, Shanghai, China.

*Corresponding authors: gerottoamanda@alumni.usp.br, zhh@ethz.ch

Abstract

Understanding the variations in past ocean carbonate chemistry is critical to elucidating the role of the oceans in balancing the global carbon cycle. The fossil shells from marine calcifiers present in the sedimentary record are widely applied as past ocean carbon cycle proxies. However, the interpretation of these records can be challenging due to the complex physiological and ecological response to the carbonate system during an organisms' life cycle, as well as the potential for preservation at the seafloor. Here we present a new dissolution proxy based on the morphological attributes of coccolithophores from the Noëlaerhabdaceae family (*Emiliania huxleyi* and *Gephyrocapsa* spp., > 2 μm). To evaluate the influences of coccolithophore calcification and coccolith preservation on fossil morphology, we measured morphological attributes, mass, length, thickness, and shape factor (ks), of coccoliths in a laboratory dissolution experiment and surface sediment samples from the South China Sea. The coccolith morphological data in surface sediments were also analyzed with environment settings, namely surface temperature, nutrients, pH, chlorophyll-a concentration, and carbonate saturation of bottom water by a redundancy analysis. Statistical analysis indicates that carbonate saturation of the deep ocean explains the highest proportion of variation in the morphological data instead of the environmental variables of the surface ocean. Moreover, the dissolution trajectory in the ks *vs.* length of coccoliths is comparable between natural samples and laboratory dissolution experiments, emphasizing the importance of carbonate saturation on fossil coccolith morphology. However, the mean ks alone cannot fully explain all variations observed in our work. We propose that the mean ks and standard deviation of ks (σ) over the mean ks (σ/ks) could reflect different degrees of dissolution and size-selective dissolution, influenced by the assemblage composition. By applying together with the σ/ks ratio, the ks factor of fossil coccoliths in deep ocean sediments could be a potential proxy for a quantitative reconstruction of past carbonate dissolution dynamics.

1. Introduction

The ocean's large reservoir capacity of carbon dioxide (CO_2) plays an essential role in the carbon cycle and, consequently, in controlling atmospheric CO_2 (Ridgwell and Zeebe, 2005; Wang et al., 2016). The ocean CO_2 is influenced by temperature, salinity, and biological activity, including primary production, respiration, calcification, and carbonate dissolution (Ridgwell and Zeebe, 2005; Sarmiento and Gruber, 2006; Libes, 2009; Wang et al., 2016). When CO_2 dissolves in water, the ocean becomes more acidic, decreasing pH, carbonate ion concentration, and carbonate saturation (Ω_{Ca}). The carbonate compensation depth (CCD) is the depth at which the rate of calcite dissolution is balanced by the rate of calcite supply. The CCD is usually several hundred meters deeper than the chemical lysocline, the saturation horizon of calcite, due to the kinetics of dissolution (Ridgwell and Zeebe, 2005). Whereas the photic zone is supersaturated with respect to calcite in most areas of the ocean, large areas of the deep ocean are currently undersaturated because of the increased solubility of calcite with pressure (Sulpis et al., 2018). As the ocean continues absorbing larger amounts of CO_2 from anthropogenic fuel emissions, a shallowing of the CCD is expected for the next 100 years due to the sharp decrease of carbonate saturation from surface to deep ocean (Hönisch et al., 2012; USGCRP, 2017; Sulpis et al., 2018; IPCC, 2019). Variations in the CCD on timescales from millions to several thousands of years are an important process in determining the ocean's carbonate chemistry and regulating atmospheric CO_2 (Emerson and Archer, 1990; Pälike et al., 2006). Understanding the role of physical and biogeochemical parameters in marine carbonates is therefore critical to interpret the geological record correctly and to reconstruct variations in the ocean carbon cycle in the past.

The effects of carbonate chemistry changes and variations in the position of the CCD in the geological past have been investigated using a wide array of geochemical and microfossil proxies such as $\delta^{13}C$ in benthic and planktonic foraminifera (Zachos et al., 2005; Hönisch et al., 2012), fragmentation indices of calcareous microfossils (Le and Shackleton, 1992; Broerse et al., 2000; Flores et al., 2003), and $CaCO_3$ content (Archer et al., 2000; Palike et al., 2006) in marine sediments. However, these proxies do not provide quantitative estimates of past changes in carbonate chemistry because some additional ecological mechanisms determine the calcification and preservation responses (Hönisch et al., 2012; Rae et al., 2021). $\delta^{11}B$ provides a quantitative proxy for past seawater pH (Hönisch et al., 2012), albeit additional carbonate chemistry parameters impose some limits on the interpretation of the proxy (Yu and Elderfield, 2007; Rae et al., 2021). Benthic B/Ca provides a quantitative proxy for deep sea CO_3^{-2} concentration (Yu et al., 2016). Yet both of these methods require mono-specific foraminifera

samples for measurements, which are time-consuming to pick, and analyses are limited to sediment samples that contain sufficient concentration of this microfossil group.

Coccolithophores, a group of single-celled calcifying algae, are characterized by the production of calcite plates called coccoliths. Coccoliths are the main constituent of marine biogenic sediments, contributing up to 80 % of deep-sea carbonate fluxes (Young and Ziveri, 2000; Hay, 2004). Changes in coccoliths morphology, distribution, and abundances are believed to record the evolution history of coccolithophores and reflect the environmental conditions in the surface ocean (i.e. during coccolith biomineralization) (Riebesell et al., 2000; Iglesias-Rodriguez et al., 2008; Beaufort et al., 2011; Charalampopoulou et al., 2016; Rigual-Hernández et al., 2020a). Because of that, coccoliths are widely used in paleoclimate and paleoceanographic reconstructions (e.g., Bollman and Herrle, 2007; Rickaby et al., 2007; Henderiks and Pagani, 2007; Bolton et al., 2016). Several methods exist to estimate coccolithophore calcification in the fossil record. Assumed proportional length and thickness allowed for the first estimates of coccolith mass using microscope techniques (Young and Ziveri, 2000). More recent methods based on the optical properties of calcite under polarized light microscopy (circular and linear) allowed a more precise estimate of the thickness of individual coccoliths (Beaufort, 2005; Bollman et al., 2014; Fuertes et al., 2014; Johnsen and Bollmann, 2020; Beaufort et al., 2021). The optical techniques have been successfully employed in downcore records to estimate coccolithophore calcification across time and evolutionary steps (e.g., Bolton et al., 2016; Beaufort et al., 2022; Guitián et al., 2022). However, until now there has been no study that evaluates the response of calcification patterns of fossil coccolithophores to both environmental parameters controlling biomineralization in the photic zone and calcite saturation state at the depth of burial.

The South China Sea (SCS) is the largest marginal basin of the Western Pacific, characterized by very dynamic spatial environmental conditions and a steep bathymetric profile (Wang et al., 2015). Sediment records from this basin have been used to study the response of coccolithophores to different environmental variables. Previous studies found positive correlations between coccolithophore biometry from plankton samples and nutrients and light at the photic zone (Jin et al., 2016). Building on these results, but applied to the sedimentary record, Su et al. (2020) explored the dependency of coccolithophore weight and past surface ocean carbon chemistry parameters and nutrient conditions. However, it has also been demonstrated that there is intense coccolithophore dissolution above the lysocline in the SCS (Fernando et al., 2007a). More recently, a study using plankton tow material found that the degree of calcification in the coccolithophore species *Emiliania huxleyi* was insensitive to carbonate chemistry in surface waters (Jin et al. 2022a). This diversity of results calls for new

104 studies that systematically explore the drivers of coccolithophore morphology and calcification
105 in the fossil record.

106 Here, we analyzed morphological attributes of fossil coccolithophores in surface
107 sediment samples in the SCS, located across spatial environmental gradients in the surface
108 ocean, but also across a bathymetric transect related to the calcite saturation at the seafloor
109 which leads to lower calcite saturation at the seafloor in deeper sites. In addition, we evaluated
110 the morphological variations of coccoliths under different dissolution intensities in a laboratory
111 experiment. Using an automated algorithm to estimate coccolithophore calcification from
112 images taken with a microscope under cross-polarization, we show that scale-invariant
113 measures of coccolith thickness (shape factor, ks) from coccolithophores located along a depth
114 gradient in the SCS are highly correlated to the calcite saturation state at the seafloor. We
115 propose a new calibration to reconstruct past calcite saturation based on ks which would enable
116 the quantitative reconstruction of changes in the calcite saturation in the deep ocean and
117 position of the CCD in the past.

118

2. Oceanographic settings

120 The SCS is a marginal basin located in the Western Pacific, connected to the open ocean
121 by shallow passages to the north and south (Fig. 1A). The Luzon Strait in the north is the deepest
122 (~2000 m) and the principal channel for water exchange between the SCS and the Pacific through
123 the Kuroshio Current (Qu et al., 2006; Liu et al., 2011; Wan and Jian, 2014). The modern surface
124 circulation and hydrographic characteristics of the SCS are directly associated with the seasonal
125 changes promoted by the East Asian Monsoon (EAM; Wang and Li, 2009). These seasonal
126 hydrodynamic patterns control the regional sea surface temperature (SST) distribution, salinity,
127 and nutrients (Fig. 1B-E, Wang and Li, 2009). The SST latitudinal gradient is up to 2° C with an
128 annual average of 28-29° C in the southern SCS and 26-27° C in the north (Tian et al., 2010).
129 Salinity varies seasonally between 32.8-34.2 psu, with smaller salinity variation in the north than
130 in the south (Wang and Li, 2009). Northern SCS primary productivity reflects the seasonality of
131 the EAM with more productive and well-mixed waters during the winter season (Zhang et al.,
132 2016), with higher chlorophyll-a concentration (0.65 mg Chl-α m^{-3} and 600 mg C m^{-2} d^{-1}) (Chen,
133 2005; Chen et al., 2006; Jin et al., 2016).

134

135
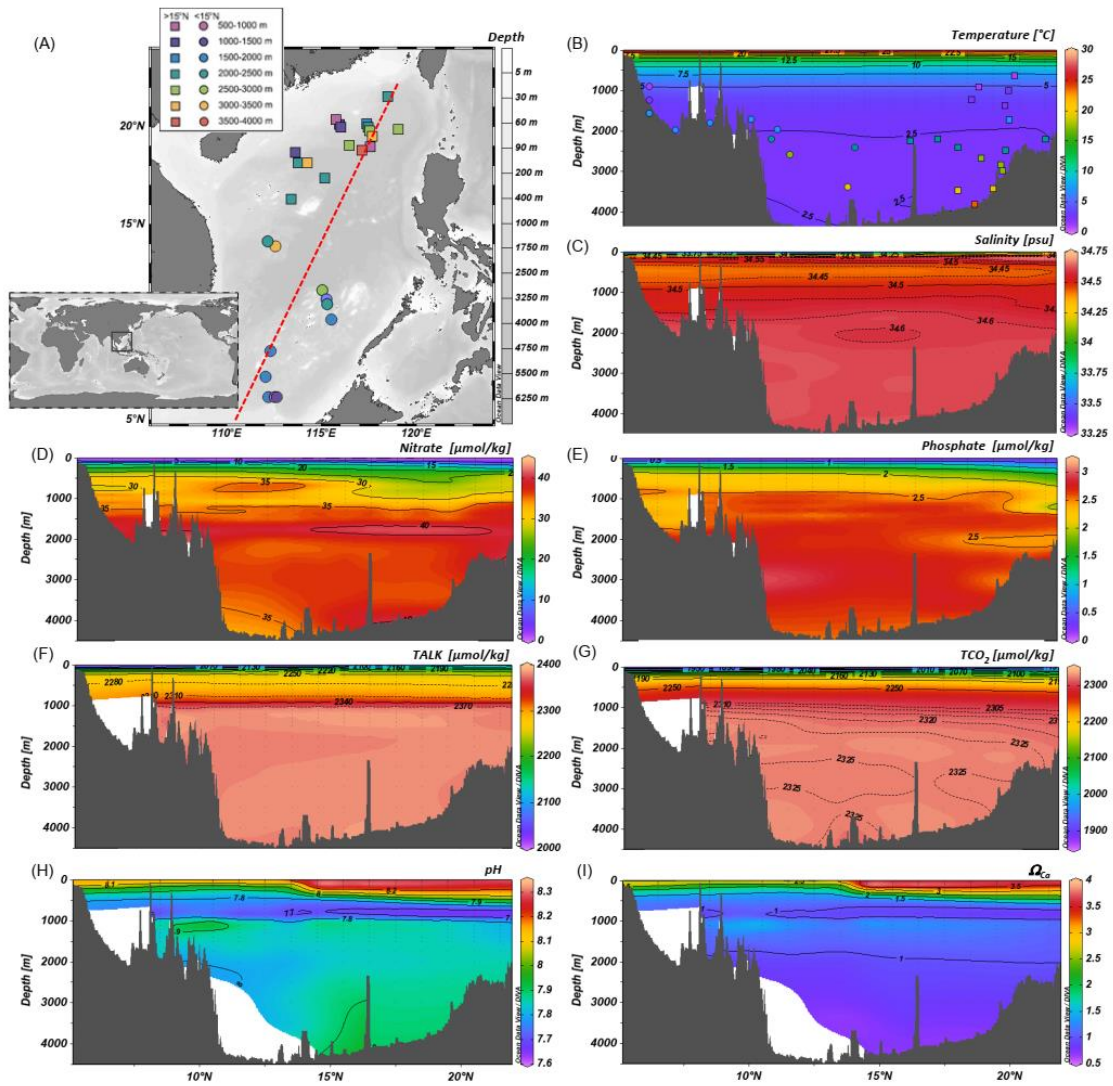
Figure 1. Map of the South China Sea and location of core-top samples used in the present study. Dots and squares represent stations located from 6° to 15° N, and from 15° to 22° N. (A). Vertical profiles along N-S (5° to 22° N) transect (dotted red line on panel A) of (B) temperature, (C) salinity, (D) nitrate, and (E) phosphate, (F) total alkalinity (TALK) and (G) total inorganic carbon concentration (TCO$_2$), (H) pH and (I) Ω_{Ca} calculated at CO2SYS (Pierrot et al., 2012). See M&M 3.3 section for data sources. The map and the vertical profiles were plotted with Ocean Data View (ODV) software (Schlitzer, 2019). Colored dots in panel (B) indicate the geographical position along the transect shown in panel (A) of the surface sediment samples used in this study.

145

The modern SCS lysocline is approximately 1200 m, and the CCD lies between 3500 and 3800 m (Thunell et al., 1992; Wang et al., 1995; Luo et al., 2018). In the northern SCS, surface waters (e.g., the upper 300 m) are characterized by relatively low DIC and TALK (Fig. 1F-G) and

149 higher pH and Ω_{Ca}, compared to deeper waters (Fig. 1H-I) (Chou et al., 2007; Jin et al., 2016).

150 Below 1000 m, the SCS across a N-S transect is characterized by relatively homogeneous DIC,

151 $\delta^{13}C$, and $[CO_3^{2-}]$ (Chen et al., 2006; Qu et al., 2006; Chou et al., 2007; Wan et al., 2020).

152   The SCS deep waters originate from the North Pacific Deep Water (NPDW) that

153 penetrates the marginal basin through the Luzon Strait (Qu et al., 2006; Liu et al., 2011; Wan

154 and Jian, 2014; Wan et al., 2018). The route traced from the Luzon Strait to the northwest

155 suggests a predominantly cyclonic deep circulation (Qu et al., 2006; Wang and Li, 2009). The

156 deep-water residence time of the SCS is estimated to be approximately 30-50 years, like that of

157 intermediate waters, 52 years (Chen et al., 2001). Due to this short residence time, the SCS

158 presents a homogeneous vertical profile; below 2000 m, there are no evident chemical

159 stratification or changes compared to the Pacific deep-water chemistry (> 2000 m)

160 characteristics (Chen et al., 2001; 2006; Qu et al., 2009). The rapid residence time potentially

161 implies that, when replaced, deep waters occupy intermediate water levels (between 300 m and

162 1300 m), contributing to the circulation of intermediate and shallow waters and ocean-

163 atmosphere exchanges (Qu et al., 2009; Tian et al., 2010).

3. Material and methods

3.1 Material and sample treatments

166   The core-top samples (n =28) employed in this study were retrieved from different

167 depths in the basin of SCS (Fig. 1) during the R/V Sonne cruises (SO-95) (Table 1). Toothpick

168 samples from each location were used to prepare smear slides, without any chemical or physical

169 treatment, following standard micropaleontological procedures (Marsaglia et al., 2015).

170 Unfortunately, the surface sediments were already depleted resulting in not having enough

171 material to perform dissolution experiments using the same samples. For the dissolution

172 experiment, we employed 240 mg of dry sediment obtained from a Late Pleistocene sample

173 from the Western Equatorial Pacific (Ocean Drilling Program -ODP- 807A-2H-2W, 57-59 cm). The

174 distribution of coccolithophore species belonging to the Noëlaerhabdaceae family in the sample

175 ODP 807 is 41% of *G. oceanica*, 34% of *G. caribbeanica* and 23% of small *Gephyrocapsa*. These

176 taxa are thicker particularly *G. caribbeanica,* than the thinner Noëlaerhabdaceae species

177 commonly found in the SCS (e.g. *E. huxleyi,* Roth and Berger, 1975; Roth and Coulbourn, 1982).

178 The sediment sample was suspended in 120 ml Milli-Q water, and then the suspension was

179 separated into 6 centrifuge tubes, each with a volume of 20 mL and containing the equivalent

180 of 40 mg of sediment. Sodium hexametaphosphate $(NaPO_3)_6$ (Calgon®) has traditionally been

181 used in pretreatment of samples with calcareous microfossils, particularly foraminifera (Olson

182 and Smart 2004; Smart et al., 2008). However, it has been observed that application of this

183 chemical agent dissolves these microfossils due to complexation of Ca with phosphates, an

184 effect which varies with the exposure time (Feldmeijer et al., 2013). Therefore, we added 100

185 mg of Calgon® into 100 ml Milli-Q water, resulting in a concentration of 1.6mM, to conduct our

186 dissolution experiment. Different volumes of Calgon® solution (0, 0.4, 0.8, 2, 4 6 ml) were added

187 to each of the six subsamples. The Calgon® is very corrosive to the fine carbonate particles, and

188 the reaction between Calgon® and carbonate could be simplified in two steps. First, the $(NaPO_3)_6$

189 hydrolysis releases the sodium trimetaphosphate $(Na_3P_3O_9)$. Then, the calcium in the solution is

190 exchanged with sodium and precipitate as $Ca(PO_3)_2$, $CaNa(PO_3)_3$, and $CaNa_4(PO_3)_6$, strongly

191 reducing the free calcium concentration in the solution. The decrease in calcium concentration

192 promotes carbonate dissolution. In theory, adding 1 mol $(NaPO_3)_6$ would result in the dissolution

193 of 3 mol $CaCO_3$ at maximum. So, there could be ~80 % carbonate left even after adding 6 ml

194 Calgon® solution. The particles in all tubes were kept suspended gently by a rotating

195 disaggregation wheel as described previously (Stoll and Ziveri, 2002) for two days to achieve a

196 full reaction between carbonate and $(NaPO_3)_6$. Slides were prepared for coccolith morphological

197 analyses using the drop technique as described by Bordiga et al. (2015) to trace the variations

198 of coccolith amount during dissolution.

199

200 3.2 Coccolith morphological parameters

201   The morphological parameters of coccoliths in the dissolution experiment and surface

202 sediment were analyzed using a Polarized Microscope (Zeiss Axio Scope HAL100), configured

203 with circularly polarized light and a Zeiss Plan-APOCHROMAT 100x/1.4 oil objective, and a

204 coupled camera (Zeiss Axiocam 506 Color). For every sample, at least 40 fields of view were

205 photographed. After species identification and selection of coccolithophores images belonging

206 to the Noëlaerhabdaceae family (*Emiliania huxleyi* and *Gephyrocapsa* spp., > 2 μm), each sample

207 had between 100 and 400 (average of 250 per sample) coccolithophore images. The relationship

208 between the color of coccolith images and thickness was calibrated using a reference calcite

209 wedge, the thickness of which had been carefully quantified (González-Lemos et al., 2018). After

210 calibration, all images were analyzed in the Matlab-based software, C-Calcita (Fuertes et al.,

211 2014), to obtain the coccolith morphological parameters, including length, volume, and mass.

212 The length-shape factor of each coccolith, ks, was calculated using the formula by Young and

213 Ziveri (2000) based on the coccolith mass and length obtained from C-Calcita:

214 $\text{ks} = \frac{Mass}{2.7 \times Length^3}$

215

216   Beyond the traditional morphological parameters, we calculated the ratio of the
217   standard deviation of ks (σ) over the mean ks (σ/ks). The goal of this novel parameter is to
218   provide a new dimension to trace the dissolution process in coccoliths, especially when the
219   coccolith assemblage is diverse. For example, if the coccoliths dissolve at different speeds in the
220   assemblage due to differential sensitivity to acidification, a small increase of σ/ks would be
221   expected at the beginning of the dissolution because of the σ increase and ks decrease. Then,
222   after all fragile coccoliths dissolve, leaving only thicker coccoliths in the assemblage, the σ/ks
223   should show a decreasing trend which could be mainly caused by a decrease σ.

224

225   Table 1. Station, coordinate data, and water depth of core-top samples used in this study.

Station	Longitude (E)	Latitude (N)	Water depth (m)
17930	115.782	20.333	629
17965	112.552	6.157	889
17943	117.553	18.95	917
17931	115.963	20.1	1005
17944	113.637	18.658	1219
17963	112.667	6.167	1233
17932	116.037	19.952	1365
17964	112.213	6.158	1556
17960	115.558	10.12	1707
17940	117.383	20.117	1728
17961	112.332	8.507	1795
17959	115.287	11.138	1957
17962	112.082	7.182	1970
17949	115.167	17.348	2195
17957	115.31	10.9	2197
17941	118.483	21.517	2201
17951	113.41	16.288	2340
17945	113.777	18.127	2404
17955	112.177	14.122	2404
17939	117.455	19.97	2473
17958	115.082	11.622	2581
17934	116.462	19.032	2665
17938	117.538	19.787	2835

17925	119.047	19.853	2980
17956	112.588	13.848	3387
17937	117.665	19.5	3428
17946	114.25	18.125	3465
17936	117.12	18.767	3809

226

227

228   3.3 Environmental data for surface sediment

229   Annual means of different physical, chemical and biological variables in both 50 m depth

230   and bottom water for the location of the surface samples (Table 1) were extracted from different

231   databases, interpolated to the geographical location of the surface sediment samples. Here the

232   50 m depth was selected because it is the depth at which the highest concentration of

233   Noëlaerhabdaceae coccolithophorid is observed in the SCS (Jin et al., 2016). Seawater

234   temperature, salinity, nitrate, and phosphate concentrations at 50 m were obtained from

235   WOA01 (Fig. 1B,C,D,E). Sea surface chlorophyll-a concentration data were based on MODIS data

236   (2003-2016) extracted from Oregon State University Ocean Productivity

237   (http://www.science.oregonstate.edu/ocean.productivity/). Annual averaged concentrations of

238   total alkalinity (TALK) and dissolved inorganic carbon (TCO_2) were extracted from Goyet et al.

239   (2000) (Fig. 1F,G). Then the carbonate ion concentration, Ph (Fig. 1H), pCO_2 for the depth of 50

240   m and Ω_{Ca} for the seafloor depth were calculated by CO2SYS macro for Excel® (Pierrot et al.,

241   2012) (Fig. 1I) using salinity, temperature, pressure, total phosphate, total silicate, TALK, and

242   TCO_2 at the corresponding depth (50 m or depth of the surface sediment sample). The light

243   intensity at 50 m water depth was calculated using a model of penetration of photosynthetic

244   active radiation (PAR) from surface to depth (Buiteveld, 1995; Murtugudde et al., 2002), monthly

245   climatologies of PAR from the MODIS Ocean database (http://oceancolor.gsfc.nasa.gov/cgi/l3),

246   and the diffuse attenuation coefficient for downwelling irradiance at 490 nm (Kd490) and

247   Equation 1 in Lin et al. (2016).

248

249   3.4 Statistical analysis

250   Pearson correlation and redundancy analysis (RDA) were employed to explore the

251   relationship between morphological features of the coccoliths in surface sediment samples and

252   the environmental data. All statistical analyses were performed using the PAST 4.06 software

253   (Hammer et al., 2001).

254

4. Results

4.1 Variations of coccoliths morphology in the dissolution experiment

In the dissolution experiment, mean ks decreased with increasing volume of Calgon® solution (Fig. 2A). The mean ks varied between 0.12 (0 ml Calgon®) and 0.04 (6 ml Calgon®) (Fig. 2A). The σ/ks represents variation in preservation among coccoliths within each sample. Higher differences in σ were observed in samples containing 2 ml, 4 ml, 0.8 ml, 0.4 ml, 0 ml, and 6 ml, respectively (Fig. 2B). Increasing the amount of Calgon® solution up to 2 ml showed a decrease in mean ks and an increase in σ. Samples with 4 and 6 ml Calgon® solution showed a reduction in mean ks and σ among coccoliths (Fig. 2B). The lowest mean ks (0.04) and the maximum mean length (3.95 µm) were recorded under the higher Calgon® solution (6 ml) amount (Fig. 2C). Increased amounts of Calgon® solution also resulted in a gradual increase in coccolith length leading to a negative correlation between length and ks ($r = -0.68$, $p > 0.05$), but not significant due to the small number of observations (Fig. 2C).
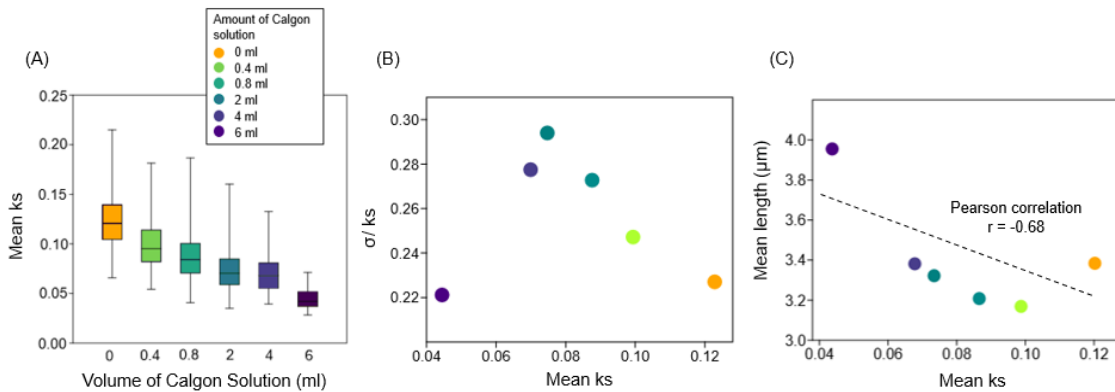
Figure 2. Coccolith morphological variations in the dissolution experiment. (A) Box plots of the median (horizontal line inside the boxes), minimal and maximal values of coccoliths mean ks (vertical bars) under the different volumes of Calgon® solution; (B) Scatter plot of mean ks and σ/ks and (C) linear correlation and correlation coefficient ($p > 0.05$) between mean ks and mean length.

4.2 Variations in coccolith morphology in natural conditions

Overall, the mean ks, thickness, and volume in the core-top sampling stations (Fig. 3) presented higher values in shallower depths. The mean ks varied between 0.03 and 0.07, and the mean thickness was between 0.25 and 0.44 µm, with maximum values recorded at station 17931 located in northern SCS at 1005 m water depth. The mean length of coccolith varied between 3.23 and 3.78 µm, with the highest values recorded at 2195 m water depth (site 17949) in northern SCS, but without a significant trend along depths. The mean volume of coccoliths ranged between 1.70 and 2.97 µm³, and the mean mass was between 4.61 and 8.03 pg, with

283   maximum values for both recorded in the shallowest station (e.g. 17930), at 629 m water depth

284   in northern SCS.
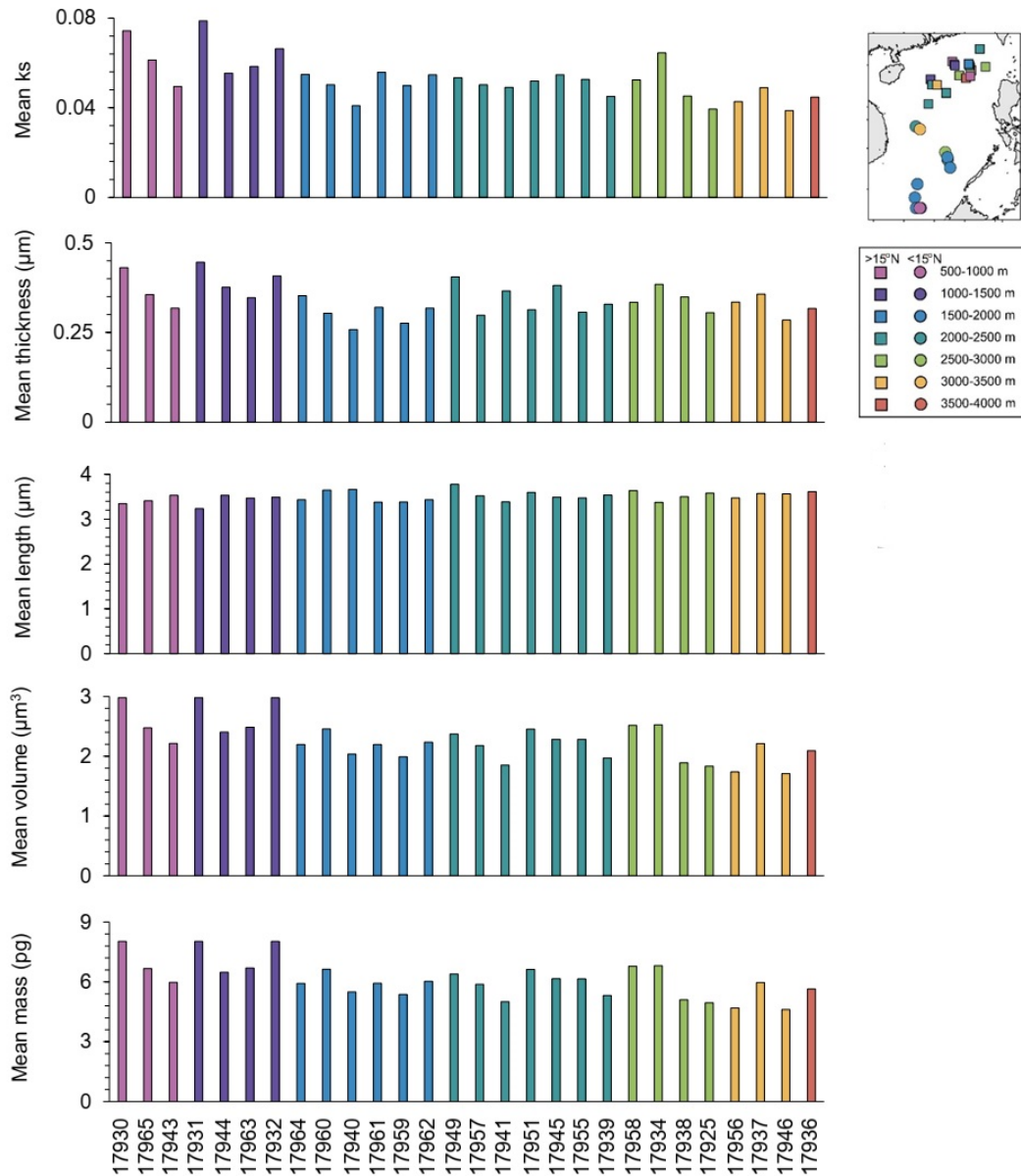
285

286   Figure 3. Coccolith mean ks, thickness (µm), length (µm), volume (µm^3), and mass (pg) in surface

287   samples from SCS. The sampling stations are distributed along the x-axis according to their

288   depth, sorted from the shallowest to the deepest.

289

290   In general, the degree of dissolution varied according to the depth of the sediment

291   samples. The calcite saturation, Ω_{Ca}, decreases with colder temperature, higher pressure and

292   higher CO_2 concentration in deep ocean. The σ/ks *vs*. ks presents different trajectories

293   associated with light, strong, or no dissolution (Fig. 4A). The shallowest stations south (<15° N)

294   and north SCS (> 15° N) show a linear and increasing trend between ks and σ/ks. For the samples

295   below 2000 m, there is no clear pattern of variation related to the mean ks standard deviation.

296 However, samples below 3000 m are mainly located on the left upper part of the plot, in a similar

297 position as the samples treated with 4 and 6 ml of Calgon® in the ks *vs*. σ/ks comparison of the

298 dissolution experiment (Fig. 3B). The mean ks *vs*. mean length shows a negative correlation (r =

299 -0.62, p < 0.05), with the deepest samples showing larger size coccoliths and lower mean ks (Fig.

300 4B).

301

302
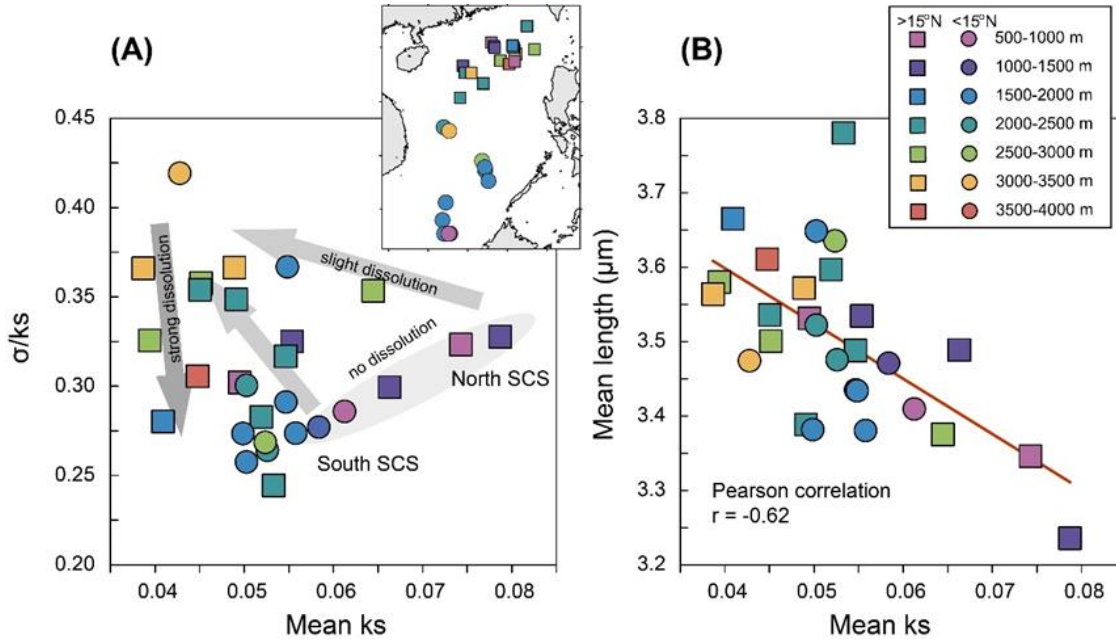
304 Figure 4. Morphological parameters of coccolith in surface sediments (A) Scatter plot between

305 mean ks and σ/ks and (B) linear correlation and correlation coefficient (p < 0.05) between mean

306 ks and mean length. Shaded arrows in panel A represent ideal trajectories of mean ks *vs*. σ/ks

307 as shown in figure 2B, to interpret the trends in the surface sediment samples. Note that the

308 mean ks of figures 2 and 4 are different due to the higher abundance of the species *G.*

309 *caribbeanica,* with higher thickness, in the sample for the dissolution experiment.

310

311   We analyzed the correlations between the biological and environmental datasets (Table

312 2). Although some of the surface variables were autocorrelated, they were included in our

313 analyses because some studies have identified a strong influence of these parameters on

314 coccolith morphology during the life-cycle (e.g. Chen et al., 2007; Jin et al., 2016). Significant

315 correlations can be found (p < 0.05) between several morphological parameters of coccolith and

316 bottom water carbonate chemistry (Ω_{Ca}), with a correlation coefficient (r) = 0.67 between mean

317 ks and Ω_{Ca}, r = 0.66 between mean volume and $\Omega_{Ca,}$ and r = 0.66 between mass and $\Omega_{Ca.}$ The

318 mean thickness of the coccolith shows a significant correlation with Ω_{Ca} at the sample depth (r

319   = 0.41), and with the concentrations of nutrients nitrate and phosphate at 50 m (r = 0.44 and

320   0.4, respectively). Surprisingly, the mean length showed no significant correlation to any

321   environmental variables except with PAR (r = 0.35).

322   The results of RDA can provide another critical perspective on the control of

323   environmental variables on coccolith morphology. The RDA1 and RDA2 explain together 58.3 %

324   of the total variations in coccolith morphological data. The surface sediment samples, color-

325   coded by different depth intervals, are distributed along the axis of RDA1, which is the most

326   important and explains 54.6 % of the total variance (Fig. 5A). Among the environmental

327   variables, Ω_{Ca} shows the highest correlation to RDA1 (r = -0.67, p < 0.05). The results of both the

328   correlation analyses and the RDA show that Ω_{Ca} in bottom water is the most important

329   environmental variable driving the morphological dataset, which shows a high correlation with

330   mean ks (r= 0.69; p < 0.05) and could explain up to 47 % (R^2= 0.47) of the variance observed in

331   mean ks (Fig. 5B). The RDA2 explained 3.69 % of the variance and is mainly correlated to the

332   salinity, temperature, pH, phosphate, TALK, and pCO_2 (Fig. 5A). The null response of coccolith

333   length to any environmental parameter is also observed in the RDA plot by its position near the

334   center of the ordination space, significantly contrasting with other morphological parameters

335   (Fig. 5A).

336

337   Table 2. Correlation matrix (p-value and Pearson correlation) between biological and

338   environmental variables. Bold values indicate significant correlations (with p < 0.05).

Environmental/ Biological	p value					r				
	Mean ks	Mean thickness	Mean length	Mean volume	Mean mass	Mean ks	Mean thickness	Mean length	Mean volume	Mean mass
Salinity	0.79	0.07	0.87	0.86	0.86	-0.05	0.34	0.03	-0.03	-0.03
Temperature	0.94	0,04	1.0	0.90	0.90	-0.01	-0.39	0.00	-0.02	-0.02
Phosphate	0.88	0.03	0.63	0.96	0.96	0.03	**0.41**	-0.09	-0.01	-0.01
Nitrate	0.36	0.02	0.30	0.71	0.71	0.17	**0.44**	-0.20	0.07	0.07
TALK	0.53	0.13	0.70	0.60	0.60	-0.12	0.28	0.07	-0.10	-0.10
Chlorophyll-a	0.26	0.18	0.88	0.18	0.18	0.22	0.25	-0.02	0.26	0.26
PAR	0.28	0.05	0.06	0.50	0.50	-0.21	-0.38	0.35	-0.13	-0.13
pH	0.18	0.31	0.38	0.24	0.24	-0.26	0.19	0.17	-0.22	-0.22
pCO_2	0.16	0.33	0.38	0.21	0.21	0.27	-0.19	-0.17	0.24	0.24
Ω_{Ca}	**0.00**	**0.03**	0.05	**0.00**	**0.00**	**0.67**	**0.41**	-0.36	**0.66**	**0.66**

339

340   TALK = total alkalinity, PAR = photosynthetic active radiation and, Ω_{Ca} = carbonate saturation.

342
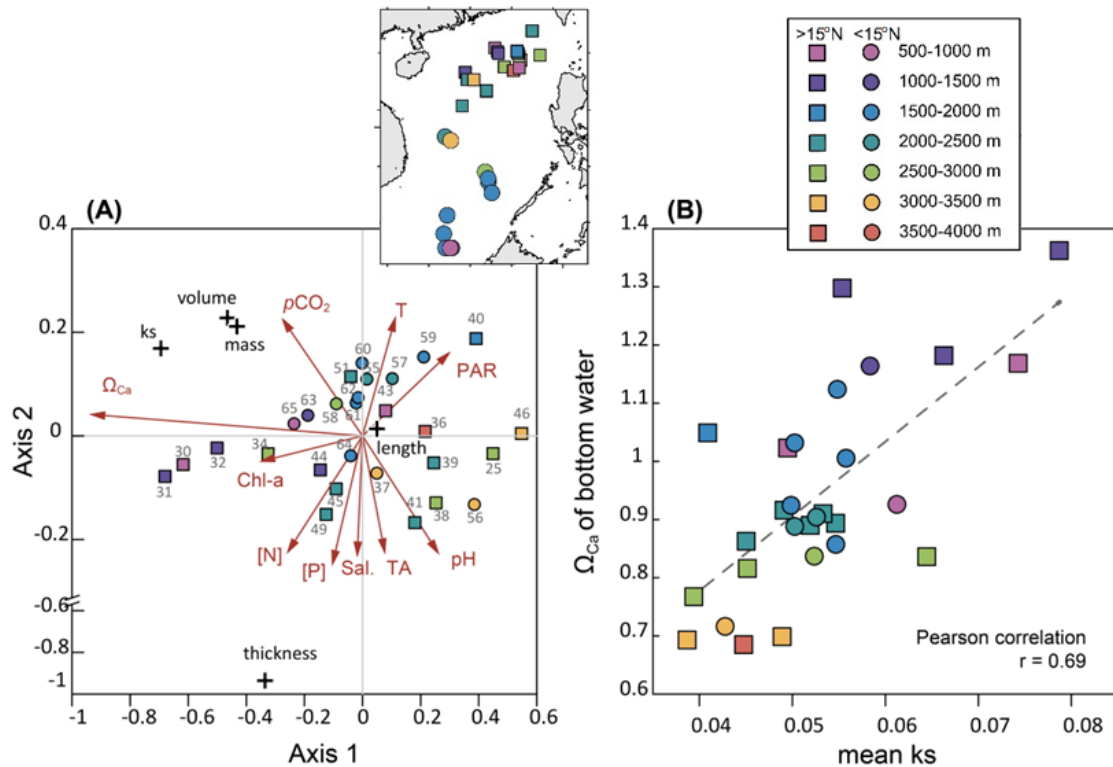
343 Figure 5. Redundancy analysis (RDA) ordinations for environmental variables and morphological

344 measurements (A) and (B) linear correlation and correlation coefficient (p < 0.05) between Ω_{Ca}

345 at bottom depths and mean ks from surface samples.

346

347 ## 5. Discussion

348 ### 5.1 Comparison between laboratory dissolution experiment and natural samples

349

350   In this study, we evaluate fossil coccolith responses to dissolution under laboratory

351 experiments and field settings. In the dissolution experiment, ks values are higher than the

352 modern coccoliths in the SCS due to the higher abundance of the relatively thicker *G.*

353 *caribbeanica* in the downcore sediment sample. Though the absolute values of ks cannot be

354 directly compared between the dissolution experiment (Fig. 2B) and surface sediments (Fig. 4A),

355 the trajectory of morphological variations during the dissolution experiment does provide

356 important diagnostic information to explain phenomena observed in the surface sediment

357 samples.

358   First, the phenomenon that coccolith length increased with the decrease of ks could be

359 observed in both the dissolution experiment (Fig. 2C) and natural surface sediments (Fig. 4B).

360 The laboratory experiment showed that under controlled conditions (known changes in water

361   chemistry and uniform species composition), the coccolith morphology variations (mean length

362   and mean ks) reflected different degrees of dissolution. We also observed a length-related

363   dissolution pattern, where smaller coccoliths gradually dissolve with the increase in Calgon®

364   concentration, leading to a higher average length but a lower mean ks. The mean ks and mean

365   length relationships in the surface samples (Fig. 4B) show a similar trend to the laboratory

366   observations (Fig. 2C). Thus, the observed trend and the largest size and lowest ks in the surface

367   sediment samples are explained by the dissolution of the smallest species due to the lower Ω_{Ca}

368   at the deepest samples and increasing the abundance of the larger coccoliths.

369   Second, changes in the σ/ks ratio in the dissolution experiment reflect a slight and

370   gradual increase in dissolution and then a decrease with the highest concentrations of Calgon®

371   (Fig. 2C). In the laboratory experiment, the subsample with no Calgon® solution presented well-

372   preserved coccoliths with high mean ks and a small standard deviation. As the amount of

373   Calgon® solution added to each subsample increases, small coccoliths start dissolving

374   preferentially, decreasing the mean ks and increasing the standard deviation (Fig. 2B). With

375   higher amounts of Calgon® solution (4 and 6 ml), the small coccoliths are completely dissolved,

376   resulting in an assemblage dominated by larger coccoliths (Fig. 2C). Under these highest

377   dissolution stages, the larger coccoliths are also partially dissolved then both mean ks and σ

378   decrease (Fig. 2B). In this way, the σ reflects how differential dissolution size selection affects

379   the composition of the assemblages. Hence, samples that are more (less) susceptible to

380   dissolution result in more homogeneous (heterogeneous) assemblages regarding carbonate

381   preservation.

382   However, the trajectory of σ/ks *vs*. ks in surface sediments seems more complex than in

383   the dissolution experiment (Fig. 4A). First, there is a group of samples with a positive correlation

384   between σ/ks and ks from shallow areas of the north and south SCS. The depth of samples from

385   northern and southern SCS regions is similar, so we argue that this feature is not caused by

386   dissolution but due to the assemblage composition differences in both parts of the SCS. The

387   coccolithophores have multi-stage blooms in the north SCS, with a peak of *G. oceanica* in late

388   winter, when coccolithophore fluxes are highest due to strong water column mixing and

389   renewed nutrient inventory, and another of *E. huxleyi* in early spring (Chen et al., 2007; Jin et

390   al., 2019). In contrast, *E. huxleyi* is the dominant species in the more oligotrophic south SCS

391   (Fernando et al., 2007b) due to its higher competitiveness in situations of lower nutrient

392   concentration (particularly nitrate) compared to *G. oceanica* (Eppley et al., 1969). So, even

393   without any influence from dissolution, the assemblages in the north SCS should feature a higher

394   species diversity and, thereby, a higher σ/ks compared with the coccolith in the south SCS.

395   Hence, the variety of the coccolith assemblages in the surface sediment samples results in

different trajectories in σ/ks *vs*. ks plotting. These results highlight the role of assemblage composition on the degree of dissolution as the large geographical variability potentially influences the coccolithophore calcite production during its life cycle. But the general trend of σ/ks *vs*. ks in surface sediment is still following the trends observed in the dissolution experiment: (1) ks decreases with dissolution; (2) σ/ks increases slightly when dissolution starts and (3) then it decreases with greater dissolution.

5.2 Sedimentary record of coccolith morphology: calcification *vs*. dissolution factors

Previous studies have evaluated changes in the calcification of Noëlaerhabdaceae coccoliths in glacial-interglacial cycles through analyses of the coccolith mass and attributed morphological variations mainly to water column nutrient availability and carbonate chemistry parameters, related to the coccolithophores life-cycle (e.g., Beaufort et al., 2011). Su et al. (2020) found that the environmental dynamics of the surface photic zone controlled Noëlaerhabdaceae coccoliths' calcification in northern SCS (MD05-2904). Similarly, higher calcite production recorded by increased coccolith mass has been attributed to the increased [CO_3^{2-}] in the surface water column in the South Indian Ocean and North Atlantic Ocean in modern sediments (Beaufort et al., 2011). Dissolution effects were thought to be less likely drivers of changes in the morphology of coccolith (Beaufort et al., 2011; Su et al., 2020), which is a reasonable assumption for the coccoliths depositing in shallow sediments above the lysocline. These interpretations are partially sustained by the findings of Beaufort et al. (2007), who found no significant coccolith dissolution during the settling in sediment traps deployed between 250 and 2500 m. The former study proposed that most of the dissolution occurs in the euphotic zone and possibly in the guts of grazers, therefore, discarding the impact of bottom water chemistry and/or post-burial processes on coccolithophore weight.

In our set of samples in the SCS, the RDA results show that mean thickness and length significantly correlate to nitrate and phosphate at 50 m (Table 2). This observation agrees with Jin et al. (2016), who found that biometric attributes of *E. huxleyi* correlated with nutrient concentrations in the plankton samples in the East China Sea (ECS). Nutrient variables are important for coccolithophore calcification (Raven and Crawfurd, 2012) and morphological parameters, at least in species of the Noëlaerhabdaceae family (Båtvik et al., 1997; Pasche et al., 1998). However, based on the extended evidence of our study, including carbonate chemistry at the depth of the sediment samples in the SCS, we observe evidence that several of the morphological parameters measured are not only influenced by primary biomineralization. Still, abiogenic post- or syn-depositional processes override this signal in the sediment samples in this

region. The highest correlations between coccolith morphology, namely mean ks, volume, and thickness, with the bottom water calcite saturation, Ω_{Ca}, indicates that the calcium carbonate preservation conditions could strongly override some of the morphological parameters in fossil coccoliths (Table 2, Fig. 5A). We suggest that the mean ks of coccolith could be a potential proxy for the carbonate dissolution in the bottom water, especially in sites near or below the lyscocline.

Carbonate dissolution may also happen within the shallow sediment (Sulpis et al., 2021; Subhas et al., 2022). Based on our current dataset and using only the morphological variations, we cannot distinguish where the dissolution happens at the time of deposition in the sediment water interface, or post-burial in the first cms of the seafloor sediment. For the deep ocean deposits with lower sedimentary rates, such as the deepest parts of the SCS (Huang and Wang, 2006), the exposure time of particles to bottom water should be longer than that along the continental slope. Thus, we suggest that the major dissolution in the deep SCS happens on the sediment-water boundary instead of within pore water. Interestingly, the ks of coccolith in the surface sediment of the ECS are much lower, as low as 0.01 (Jin et al., 2019), than those in our study, which is higher than 0.04. However, the ks of coccolith during the laboratory dissolution experiment performed by Jin et al. (2019; Fig. 9A in that study) show the same range as our measurements. The ECS samples are from the continental shelf with high sedimentary rates and organic carbon content (Jin et al., 2019). In these settings, the coccoliths continuously dissolve after being buried within the first centimeters of the seafloor sediments in response to organic matter remineralization and CO_2 release, resulting in a ~30-50 % decrease in coccolith mass (Jin et al., 2019). Therefore, the sedimentary environment has to be individually evaluated to understand which process is controlling the dissolution of coccolithophores at the seafloor. More detailed work, such as in-situ pore water chemistry measurements, would be necessary to fully reveal the fate of coccolith dissolution in different burial scenarios (Holcová and Scheiner, 2022).

Among all the morphological parameters, we find the mean ks of coccolith is a more robust dissolution proxy compared to the other measured morphological parameters. Firstly, we observe a higher correlation coefficient between mean ks of coccolith and Ω_{Ca} compared with other morphological parameters. Secondly, although volume, mass, and thickness are also highly correlated with Ω_{Ca}, these morphological parameters vary more with the feature of different coccolithophores, including variations in coccolith circularity and cell sizes (Young and Ziveri, 2000; Bolton et al., 2016). Thirdly, the thickness is a morphological pattern sensitive to the upper ocean's preservation and surface ocean nutrients conditions during biomineralization (Table 2). Another important feature of ks is its high sensitivity to dissolution. As shown in Fig.

466 4, the ks of coccolith have already begun to decrease even though the water depths are only at

467 ~2000 m, which is below the modern lysocline but above the CDD in the SCS (Wang et al., 1995;

468 Luo et al., 2018). Finally, the dissolution effects on morphological attributes of mean ks agree

469 well with the laboratory dissolution experiment, in which each subsample's mean ks reflected

470 different preservation stages (Fig. 3).

471 Despite a noticeable degree of uncertainty due to the mixing of life-cycle and post-

472 mortem signals in the sedimentary record, similar findings of calcite dissolution modifying

473 coccolith's morphology in waters at or below saturation suggest that the conclusions drawn

474 from the present study are not unique to the SCS. In the Sub-Antarctic and Antarctic zone,

475 dissolution signals affecting coccolithophores were manifested as a decrease in mass and distal

476 shield length of *E. huxleyi* coccoliths preserved in surface sediments (Rigual-Hernández et al.,

477 2020b; Vollmar et al., 2022). Based on this collective evidence, a key reasonable question could

478 be, "can the morphological variation of coccoliths be employed to trace their evolution safely,

479 or instead be a good proxy for carbonate preservation"?

480

481 5.3. Implications for interpreting the downcore history of coccolithophore
482 morphology

483 On longer time scales, the morphological variations of coccoliths have been employed

484 to trace coccolithophores evolutionary trends. Bolton et al. (2016) first measured the ks of

485 Noëlaerhabdaceae in the last 15 million years. They found that the decrease of coccolith ks

486 paralleled the reduction of atmospheric pCO_2 since the late Miocene and interpreted this as a

487 decrease in biomineralization. More recent works by Beaufort et al. (2022) and Jin et al. (2022b)

488 focused on the coccolithophore evolution over the last 2 million years by measuring coccolith

489 mass, highlighting the role of seasonality and local environments in the evolution and

490 production of Noëlaerhabdaceae. Similarly, Guitián et al. (2020) studied size trends across

491 different regions between Oligocene to the Early Miocene, concluding that cell size distribution

492 was controlled by multiple competing factors, with a strong selective pressure from CO_2 decline

493 as a potential mechanism. This study examined dissolution by looking, among others, at the

494 fragmentation and etching of coccoliths and found that temporal trends in lith size distributions

495 were not significantly affected. This agrees with our observations since the mean length in SCS

496 surface sediments does not correlate with any saturation state related parameter. However,

497 Guitián et al. (2022), using a new calibration in the C-Calcita software that enables estimations

498 of coccolith thickness up to 3.1 microns, found that elliptical ks (kse) was inversely correlated

499 with the relative abundance of dissolution-resistant nannoliths. This was interpreted as a

500 dissolution control on the elliptical shape factors in coccolithophores between Oligocene and

501 Miocene, as it was found in our surface sediment samples. Therefore, we propose that for

502 studies focusing on coccolithophore evolutionary histories, it would be safer to select a shallow

503 sediment core with low organic carbon content, high clay content, and always lying above the

504 carbonate lysocline (Guitián et al., 2020).

505   One useful way to identify dissolution in these studies covering geological time scales

506 could be plotting the σ/ks against ks. If an increase of σ/ks is detected in the sediment coccolith

507 without any significant variations in coccolith assemblage or with an increase in dissolution-

508 resistant species (Guitián et al., 2022), it should be interpreted as dissolution. Another way to

509 determine separate evolutionary/ecological influences on ks variations could be to measure the

510 ks of coccolith across a close spatial gradient which includes different depositional depths.

511 Significant variations in the morphological attributes of the fossil coccolithophores would likely

512 be caused by different saturation through time at different sites. Related to this last suggestion,

513 coupling downcore morphological assessment in coccolithophores with other calcareous

514 proxies measurements, such as size-normalized weight of planktic foraminiferal tests (Lohman,

515 1995; Broecker and Clark, 2001; Barker et al., 2002), which include recent advances in

516 morphological analyses in large microfossils (Iwasaki et al., 2015; 2019), may provide an even

517 more precise and safe quantitative estimates of past deep-carbonate chemistry parameters.

518 6. Summary

519   This study demonstrates, based on morphological attributes of *E. huxleyi* and

520 *Gephyrocapsa* spp. (> 2 µm), that dissolution effects primarily affect the morphology of

521 coccoliths preserved in the deep ocean. In the SCS surface sediments, bottom water Ω_{ca}

522 saturation plays a major role in the variation of the coccoliths' ks shape factor, which has the

523 potential, based on the current calibration, to quantitatively reconstruct past carbonate

524 dissolution changes. Our laboratory-controlled dissolution results show that the mean ks

525 decreased in response to increased amounts of corrosive solution. We propose the ratio σ/ks

526 *vs*. mean ks to evaluate the degree of dissolution (light, strong, or no dissolution) occurring in

527 the sedimentary record. A length-related dissolution pattern was also observed in the laboratory

528 and surface sediments, with small coccoliths more prone to dissolution, increasing larger

529 coccolith specimens and affecting the assemblage composition. As in the laboratory experiment,

530 the coccolith's ks from surface sediments decreased with dissolution, and the σ/ks trajectory

531 reflected different dissolution stages. However, the σ/ks in surface sediment showed a more

532 complex response due to the natural variability of the surface sediment samples in terms of

533 geographical differences in multiple environmental factors. These findings demonstrate that,

534 despite the complementary of the carbonate system and ecological aspects, the coccoliths ks

535 factor allied to σ/ks ratio has potential as a dissolution proxy to track changes in the seafloor
536 carbonate saturation state. Although a stable proxy, the mean ks should be applied with caution,
537 particularly when applied to longer time scales, in which evolutionary trends might exert control
538 on morphological attributes of fossil coccolithophores.

539 Author contributions
540 AG, HZ, RHN and IHA conceived and designed the study. AG and HZ conducted the lab work and
541 sample analyses. AG, HZ and IHA performed the statistical analysis. AG, HZ and IHA wrote the
542 manuscript with substantial contributions from all co-authors.

543 Competing interests
544 The authors declare that they have no conflict of interest.

545 Data availability
546 Research data is available as supplementary material and in the Zenodo
547 (https://doi.org/10.5281/zenodo.7271441, Gerotto et al., 2022) and PANGAEA
548 (https://doi.pangaea.de/10.1594/PANGAEA.954015 and
549 https://doi.pangaea.de/10.1594/PANGAEA.954016, Gerotto et al., 2023a,b) data repositories.

550 Acknowledgments

551 This study was financed in part by the Coordenação de Aperfeiçoamento de Pessoal de Nível
552 Superior - Brasil (CAPES) - Finance Code 001 to A.G. and the ETH Core and Swiss National Science
553 Foundation (Award 200021_182070) funding to H. M. Stoll. Additional funding was provided by
554 the National Natural Science Foundation of China (grants 42188102 and 41930536) to C.L.
555 Thanks also to the International Ocean Discovery program for providing the sample used for the
556 dissolution experiment.

557 References

558 Archer, D., Winguth, A., Lea, D., and Mahowald, N. What caused the glacial/interglacial
559   atmospheric pCO_2 cycles? Rev. Geophys., 38(2), 159–189,
560   https://doi.org/10.1029/1999RG000066, 2000.
561 Barker, S., and Elderfield, H. Foraminiferal calcification response to glacial-interglacial changes
562   in atmospheric CO_2, Science, 297(5582), 833-836,
563   https://doi.org/10.1126/science.1072815, 2002.
564 Båtvik, H., Heimdal, B. R., Fagerbakke, K. M., Green, J. C. Effects of unbalanced nutrient regime
565   on coccolith morphology and size in *Emiliania huxleyi* (Prymnesiophyceae), Eur. J.
566   Phycol., 32(2), 155–165, https://doi.org/10.1080/09670269710001737089, 1997.

567 Beaufort, L. Weight estimates of coccoliths using the optical properties (birefringence) of calcite,
568   Micropaleontology, 51(4), 289-297, https://doi.org/10.2113/gsmicropal.51.4.289,
569   2005.

570 Beaufort, L., Gally, Y., Suchéras-Marx, B., Ferrand, P., and Duboisset, J. A universal method for
571   measuring the thickness of microscopic calcite crystals, based on bidirectional circular
572   polarization, Biogeosciences, 18(3), 775-785, https://doi.org/10.5194/bg-18-775-2021,
573   2021.

574 Beaufort, L., Probert, I., De Garidel-Thoron, T., Bendif, E. M., Ruiz-Pino, D., Metzl, N., et al.
575   Sensitivity of coccolithophores to carbonate chemistry and ocean acidification, Nature,
576   476, 80–83, https://doi.org/10.1038/nature10295, 2011.

577 Beaufort, L., Probert, I., and Buchet, N. Effects of acidification and primary production on
578   coccolith weight: Implications for carbonate transfer from the surface to the deep
579   ocean, Geochem., Geophy., Geosy., 8(8), 1–18,
580   https://doi.org/10.1029/2006GC001493, 2007.

581 Beaufort, L., Bolton, C. T., Sarr, A. C., et al. Cyclic evolution of phytoplankton forced by changes
582   in tropical seasonality, Nature, 601, 79–84, https://doi.org/10.1038/s41586-021-04195-
583   7, 2022.

584 Bollmann, J. Weight approximation of coccoliths using a circular polarizer and interference
585   colour derived retardation estimates – (The CPR Method), Biogeosciences, 11, 1899-
586   1910, https://doi.org/10.5194/bg-11-1899-2014, 2014.

587 Bollmann, J., Herrle, J. O. Morphological variation of *Emiliania huxleyi* and sea surface salinity,
588   Earth Planet. Sc. Lett., 255(3-4), 273–288, https://doi.org/10.1016/j.epsl.2006.12.029,
589   2007.

590 Bolton, C. T., Hernández-Sánchez, M. T., Fuertes, M. Á., González-Lemos, S., Abrevaya, L.,
591   Mendez-Vicente, A., et al. Decrease in coccolithophore calcification and CO_2 since the
592   middle Miocene, Nat. Commun., 7, 10284, https://doi.org/10.1038/ncomms10284,
593   2016.

594 Bordiga, M., Bartol, M., Henderiks, J. Absolute nannofossil abundance estimates: 314
595   Quantifying the pros and cons of different techniques, Rev. de Micropaleontol., 58, 155-
596   165, https://doi:10.1016/j.revmic.2015.05.002, 2015.

597 Broecker, W. S., and Clark, E. Glacial-to-Holocene Redistribution of Carbonate Ion in the Deep
598   Sea, Science, 294(5549), 2152–2155, http://www.jstor.org/stable/3085356, 2001.

599 Broerse, A. T. C., Ziveri, P., and Honjo, S. Coccolithophore (-$CaCO_3$) flux in the Sea of Okhotsk:
600   Seasonality, settling and alteration processes, Mar. Micropaleontol., 39(1–4), 179–200,
601   https://doi.org/10.1016/S0377-8398(00)00020-7, 2000.

602   Buiteveld, H. A model for calculation of diffuse light attenuation (PAR) and Secchi depth, Neth.

603   J. Aquat. Ecol., 29, 55–65, https://doi.org/10.1007/BF02061789, 1995.

604   Charalampopoulou, A., Poulton, A. J., Bakker, D. C. E., Lucas, M. I., Stinchcombe, M. C., Tyrrell,

605   T. Environmental drivers of coccolithophore abundance and calcification across Drake

606   Passage (Southern Ocean), Biogeosciences, 13, 5917–5935, https://doi.org/10.5194/bg-

607   13-5917-2016, 2016.

608   Chen, C. T. A., Wang, S. L., Chou, W. C., and Sheu, D. D. Carbonate chemistry and projected future

609   changes in pH and CaCO3 saturation state of the South China Sea, Mar. Chem., 101(3–

610   4), 277–305, https://doi.org/10.1016/j.marchem.2006.01.007, 2006.

611   Chen, C. T. A., Wang, S. L., Wang, B. J., and Pai, S. C. Nutrient budgets for the South China sea

612   basin, Mar. Chem., 75(4), 281–300, https://doi.org/10.1016/S0304-4203(01)00041-X,

613   2001.

614   Chen, Y. L. L. Spatial and seasonal variations of nitrate-based new production and primary

615   production in the South China Sea, Deep-Sea Res. Pt. I, 52(2), 319–340,

616   https://doi.org/10.1016/j.dsr.2004.11.001, 2005.

617   Chen, Y. L. L., Chen, H. Y., and Chung, C. W. Seasonal variability of coccolithophore abundance

618   and assemblage in the northern South China Sea, Deep-Sea Res. Pt. II: Top. Stud.

619   Oceanogr., 54(14–15), 1617–1633, https://doi.org/10.1016/j.dsr2.2007.05.005, 2007.

620   Chou, W. C., Sheu, D. D., Lee, B. S., Tseng, C. M., Chen, C. T. A., Wang, S. L., and Wong, G. T. F.

621   Depth distributions of alkalinity, TCO_2 and $\delta^{13} CTCO_2$ at SEATS time-series site in the

622   northern South China Sea, Deep-Sea Res. Pt. II: Top. Stud. Oceanogr., 54(14–15), 1469–

623   1485, https://doi.org/10.1016/j.dsr2.2007.05.002, 2007.

624   Conkright, M. E., Locarnini, R. A., Garcia, H. E., O'Brien, T. D., Boyer, T. P., Stephens, C., Antonov,

625   J. I. World Ocean Atlas 2001: Objective Analyses, Data Statistics, and Figures, CD-ROM

626   Documentation. National Oceanographic Data Center, Silver Spring, MD, 17 pp, 2002.

627   Emerson, S. R., and Archer, D. Calcium carbonate preservation in the ocean. Philos. Tr. R. Soc. S-

628   A., 331(1616), 29–40, https://doi.org/10.1098/rsta.1990.0054, 1990.

629   Eppley, R. W., Rogers, J. N., and Mccarthy, J. J. Half-saturation constants for uptake of nitrate

630   and ammonia, Liminol. Oceanogr., 14(6), 912–920,

631   https://doi.org/10.4319/lo.1969.14.6.0912, 1969.

632   Feldmeijer, W., Metcalfe, B., Scussolini, P., and Arthur, K. The effect of chemical pretreatment of

633   sediment upon foraminiferal-based proxies, Geochem., Geophy., Geosy., 14(10), 3996-

634   4014, https://doi.org/10.1002/ggge.20233, 2013.

635 Fernando, A. G. S, Peleo-Alampay, A. M., Lucero, E. S., and Wiesner, M. G. Surface sediment
636    distribution of *Florisphaera profunda* in the South China Sea: an effect of dissolution? J.
637    Nannoplankton Res., 29(2), 102–07, 2007a.

638 Fernando, A. G. S., Peleo-Alampay, A. M., and Wiesner, M. G. Calcareous nannofossils in surface
639    sediments of the eastern and western South China Sea, Mar. Micropaleontol., 66, 1–26,
640    https://doi.org/10.1016/j.marmicro.2007.07.003, 2007b.

641 Flores, J. A., Marino, M., Sierro, F. J., Hodell, D. A., and Charles, C. D. Calcareous plankton
642    dissolution pattern and coccolithophore assemblages during the last 600 kyr at ODP Site
643    1089 (Cape Basin, South Atlantic): Paleoceanographic implications. Palaeogeogr
644    Palaeocl., 196(3–4), 409–426, https://doi.org/10.1016/S0031-0182(03)00467-X, 2003.

645 Fuertes, M. Á., Flores, J. A., and Sierro, F. J. The use of circularly polarized light for biometry,
646    identification and estimation of mass of coccoliths, Mar. Micropaleontol., 113, 44–55,
647    https://doi.org/10.1016/j.marmicro.2014.08.007, 2014.

648 Gerotto, A., Zhang, H., Nagai, R. H., Stoll, H. M., Figueira, R. C. L., Chuanlian, L., Hernández-
649    Almeida, I. Morphological measurements of coccoliths from surface samples of South
650    China Sea, Zenodo [data set], https://doi.org/10.5281/zenodo.7271441, 2022.

651 Gerotto, A., Zhang, H., Nagai, R. H., Stoll, H. M., Figueira, R. C. L., Chuanlian, L., Hernández-
652    Almeida, I. Morphological measurements of coccoliths from surface samples of R/V
653    SONNE cruise SO95. PANGAEA, https://doi.pangaea.de/10.1594/PANGAEA.954015,
654    2023a.

655 Gerotto, A., Zhang, H., Nagai, R. H., Stoll, H. M., Figueira, R. C. L., Chuanlian, L., Hernández-
656    Almeida, I. Coccolith dissolution experiment from one sample of ODP Hole 130-
657    807A. PANGAEA, https://doi.pangaea.de/10.1594/PANGAEA.954016, 2023b.

658 González-Lemos, S., Guitián, J., Fuertes, M. Á., Flores, J. A., and Stoll, H. M. Technical note: An
659    empirical method for absolute calibration of coccolith thickness, Biogeosciences, 15(4),
660    1079–1091, https://doi.org/10.5194/bg-15-1079-2018, 2018.

661 Goyet, C., Healy, R. J., and Ryan, J. P. Global distribution of total inorganic carbon and total
662    alkalinity below the deepest winter mixed layer depths. ORNL/CDIAC-127, NDP-076.
663    Carbon Dioxide Information Analysis Center, Oak Ridge National Laboratory, U.S.
664    Department of Energy, Oak Ridge, Tennessee, 2000.

665 Guitián, J., Dunkley Jones, T., Hernández-Almeida, I., Löffel, T., and Stoll, H. M. Adaptations of
666    coccolithophore size to selective pressures during the Oligocene to Early Miocene high
667    CO_2 world, Paleoceanogr. and Paleoclimatology, 35(12), e2020PA003918,
668    https://doi.org/10.1029/2020PA003918, 2020.

669 Guitián, J., Fuertes, M. Á., Flores, J. A., Hernández-Almeida, I., and Stoll, H. Variation in
670   calcification of Reticulofenestra coccoliths over the Oligocene-Early Miocene, Biogeosci.
671   Discuss., 1-17, https://doi.org/10.5194/bg-19-5007-2022, 2022.

672 Hammer, Ø., Harper, D. A. T., Ryan, P. D. PAST: Paleontological Statistics Software Package for
673   Education and Data Analysis, Palaeonto. Electron., 4(1), 1–9,
674   doi.org/10.1016/j.bcp.2008.05.025, 2001.

675 Hay, W. W. Carbonate fluxes and calcareous nannoplankton.
676   H. Thierstein, J. Young (Eds.), Coccolithophores: From Molecular Processes to Global
677   Impact, Springer, Berlin (2004), pp. 509-528, 2004.

678 Henderiks, J., and Pagani, M. Refining ancient carbon dioxide estimates: Significance of
679   coccolithophore cell size for alkenone-based pCO_2 records, Paleoceanography, 22(3), 1–
680   12, https://doi.org/10.1029/2006PA001399, 2007.

681 Hernández, A. S. R., Trull, T. W., Nodder, S. D., Flores, J. A., Bostock, H., Abrantes, F., et al.
682   Coccolithophore biodiversity controls carbonate export in the Southern Ocean,
683   Biogeosciences, 17(1), 245–263, https://doi.org/10.5194/bg-17-245-2020, 2020.

684 Holcová, K., and Scheiner, F. An experimental study on post-mortem dissolution and overgrowth
685   processes affecting coccolith assemblages: A rapid and complex process, Geobiology,
686   00, 1–17, https://doi.org/10.1111/gbi.12528, 2022.

687 Hönisch, B., Ridgwell, A., Schmidt, D. N., Thomas, E., Gibbs, S. J., Sluijs, A., et al. The geological
688   record of ocean acidification, Science, 335(6072), 1058–1063,
689   https://doi.org/10.1126/science.1208277, 2012.

690 Huang, W., and Wang, P. Sediment mass and distribution in the South China Sea since the
691   Oligocene. Sci. China Ser. D Earth Sci. 49, 1147–1155. https://doi:10.1007/s11430-006-
692   2019-4, 2006.

693 Iglesias-Rodriguez, M. D., Halloran, P. R., Rickaby, R. E. M., Hall, I. R., Colmenero-Hidalgo, E.,
694   Gittins, J. R., et al. Phytoplankton calcification in a high-CO_2 world, Science, 320(5874),
695   336–340, https://doi.org/10.1126/science.1154122, 2008.

696 IPCC: Climate Change and Land: an IPCC special report on climate change, desertification, land
697   degradation, sustainable land management, food security, and greenhouse gas fluxes in
698   terrestrial ecosystems [P.R. Shukla, J. Skea, E. Calvo Buendia, V. Masson-Delmotte, H.-
699   O. Pörtner, D. C. Roberts, P. Zhai, R. Slade, S. Connors, R. van Diemen, M. Ferrat, E.
700   Haughey, S. Luz, S. Neogi, M. Pathak, J. Petzold, J. Portugal Pereira, P. Vyas, E. Huntley,
701   K. Kissick, M. Belkacemi, J. Malley, (eds.)]. In press, 2019.

702   Iwasaki, S., Kimoto, K., Okazaki, Y., and Ikehara, M. Micro-CT scanning of tests of three planktic
703   foraminiferal species to clarify dissolution process and progress, Geochem., Geophy.,
704   Geosy., 20(12), 6051-6065, https://doi.org/10.1029/2019GC008456, 2019.

705   Iwasaki, S., Kimoto, K., Sasaki, O., Kano, H., Honda, M. C., and Okazaki, Y. Observation of the
706   dissolution process of *Globigerina bulloides* tests (planktic foraminifera) by X-ray
707   microcomputed   tomography, Paleoceanography, 30(4),   317-331,
708   https://doi.org/10.1002/2014PA002639, 2015.

709   Johnsen, S. L., and Bollmann, J. Segmentation, retardation and mass approximation of
710   birefringent particles on a standard light microscope, J. Microsc., 280, 30-50,
711   https://doi.org/10.1111/jmi.12932, 2020.

712   Jin, X., Liu, C., Poulton, A. J., Dai, M., and Guo, X. Coccolithophore responses to environmental
713   variability in the South China Sea: Species composition and calcite content,
714   Biogeosciences, 13(16), 4843–4861, https://doi.org/10.5194/bg-13-4843-2016, 2016.

715   Jin, X., Liu, C., Xu, J., and Guo, X. Coccolithophore abundance, degree of calcification, and their
716   contribution to particulate inorganic carbon in the South China Sea, J. Geophys. Res-
717   Biogeo., 127(4), e2021JG006657, https://doi.org/10.1029/2021JG006657, 2022a.

718   Jin, X., Liu, C., and Zhang, H. Coccolith morphological and assemblage responses to dissolution
719   in the recent sediments of the East China Sea, Mar. Micropaleontol., 152, 101709,
720   https://doi.org/10.1016/j.marmicro.2018.09.001, 2019.

721   Jin, X., Ma, W., and Liu, C. Origin of the long-term increase in coccolith size and its implication
722   for carbon cycle and climate over the past 2 Myr, Quaternary Sci. Rev., 290, 107642,
723   https://doi.org/10.1016/j.quascirev.2022.107642, 2022b.

724   Le, J., and Shackleton, N. J. Carbonate dissolution fluctuations in the western equatorial Pacific
725   during   the   late   Quaternary,   Paleoceanography,   7,   21–42,
726   https://doi.org/10.1029/91PA02854, 1992.

727   Libes, S. M. An Introduction to Marine Biogeochemistry, 2nd ed. Burlington, MA:
728   Academic Press Noone, K., Sumaila, R.; Diaz R.J. (eds) 2009. Valuing the
729   Oceans, Stockholm Environmental Institute, 2009.

730   Lin, J., Lee, Z., Ondrusek, M., and Du, K. Remote sensing of normalized diffuse
731   attenuation coefficient of downwelling irradiance, J. Geophys. Res-Oceans, 121(9),
732   6717-6730, https://doi.org/10.1002/2016JC011895, 2016.

733   Liu, J., Xiang, R., Chen, M., Chen, Z., Yan, W., and Liu, F. Influence of the Kuroshio current
734   intrusion on depositional environment in the Northern South China Sea: Evidence from
735   surface   sediment   records,   Mar.   Geol.,   285(1–4),   59–68,
736   https://doi.org/10.1016/j.margeo.2011.05.010, 2011.

737   Lohman, G. P. A model for variation in the chemistry of planktonic foraminifera due to secondary
738   calcification and selective dissolution, Paleoceanogr. Paleoclimatol., 10(3), 445-457,
739   https://doi.org/10.1029/95PA00059, 1995.

740   Luo, Y., Kienast, M., and Boudreau, B. P. Invariance of the carbonate chemistry of the South
741   China Sea from the glacial period to the Holocene and its implications to the Pacific
742   Ocean   carbonate   system,   Earth   Planet.   Sci.   Lett.,   492,   112–120,
743   https://doi.org/10.1016/j.epsl.2018.04.005, 2018.

744   Marsaglia, K., Milliken, K., Leckie, R., M., Tentori, D., Doran, L. IODP Smear Slide Digital Reference
745   for Sediment Analysis of Marine Mud. Part 2: Methodology and Atlas of Biogenic
746   Components. IODP Technical Note 2, doi:10.14379/iodp.tn.2.2015, 2015.

747   Murtugudde, R., Beauchamp, J., McClain, C. R., Lewis, M., and Busalacchi, A. Effects of
748   penetrative radiation on the upper tropical ocean circulation, J. Climate, 15(5), 470-486,
749   https://doi.org/10.1175/1520-0442(2002)015<0470:EOPROT>2.0.CO;2, 2002.

750   Paasche, E. Roles of nitrogen and phosphorus in coccolith formation in *Emiliania huxleyi*
751   (Prymnesiophyceae),   Eur.   J.   Phycol.,   33(1),   33-42,
752   https://doi.org/10.1080/09670269810001736513, 1998.

753   Pälike, H., Lyle, M. W., Nishi, H., Raffi, I., Ridgwell, A., Gamage, K., et al. A Cenozoic record of the
754   equatorial Pacific carbonate compensation depth, Nature, 488(7413), 609–614,
755   https://doi.org/10.1038/nature11360, 2012.

756   Pälike, H., Norris, R. D., Herrle, J. O., Wilson, P. A., Helen, K., Lear, C. H., et al. The heartbeat of
757   the   Oligocene   climate   system,   Science,   314(5807),   1894–1898,
758   https://www.jstor.org/stable/20035092, 2006.

759   Pierrot, D., Lewis, E., and Wallace, D. W. R. MS Excel Program Developed for CO_2 System
760   Calculations - version 2.1. ORNL/CDIAC-105a. Carbon Dioxide Information Analysis
761   Center, Oak Ridge National Laboratory, U.S. Department of Energy, Oak Ridge,
762   Tennessee, https://doi.org/10.3334/CDIAC/otg.CO2SYS_XLS_CDIAC105a, 2012.

763   Pinxian, W., Qiubao, M., Yunhua, B., and Wenke, F. Planktonic foraminifera in the continental
764   slope of the northern South China Sea during the last 130,000 years and their paleo-
765   oceanographic   implications,   Acta   Geol.   Sin-Engl.,   60(3),   1–11,
766   https://doi.org/10.1111/j.1755-6724.1986.mp60003001.x, 1986.

767   Qu, T., Girton, J. B., and Whitehead, J. A. Deepwater overflow through Luzon Strait, J. Geophys.
768   Res., 111(C1), C01002, https://doi.org/10.1029/2005JC003139, 2006.

769   Qu, T., Song, Y. T., and Yamagata, T. An introduction to the South China Sea throughflow: Its
770   dynamics, variability, and application for climate, Dynam. Atmos. Oceans, 47(1–3), 3–
771   14, https://doi.org/10.1016/j.dynatmoce.2008.05.001, 2009.

772   Rae, J. W. B., Zhang, Y. G., Liu, X., Foster, G. L., Stoll, H. M., and Whiteford, R. D. M. Atmospheric
773   CO_2 over the past 66 million years from marine archives, Annu. Rev. Earth Pl. Sc., 49,
774   609–641, https://doi.org/10.1146/annurev-earth-082420-063026, 2021.

775   Raven, J. A., and Crawfurd, K. Environmental controls on coccolithophore calcification. Mar. Ecol.
776   Prog. Ser., 470, 137–166. http://www.jstor.org/stable/24876210, 2012.

777   Rickaby, R. E. M., Bard, E., Sonzogni, C., Rostek, F., Beaufort, L., Barker, S., et al. Coccolith
778   chemistry reveals secular variations in the global ocean carbon cycle? Earth Planet. Sci.
779   Lett., 253(1–2), 83–95, https://doi.org/10.1016/j.epsl.2006.10.016, 2007.

780   Ridgwell, A., and Zeebe, R. E. The role of the global carbonate cycle in the regulation and
781   evolution of the Earth system, Earth Planet. Sci. Lett., 234(3–4), 299–315,
782   https://doi.org/10.1016/j.epsl.2005.03.006, 2005.

783   Riebesell, U., Zondervan, I., Rost, B., Tortell, P. D, Zeebe, R. E., and Morel, F. M. M. Reduced
784   calcification of marine plankton in response to increased atmospheric CO_2, Nature, 407,
785   364–367, https://doi.org/10.1038/35030078, 2000.

786   Rigual-Hernández, A. S., Sánchez-Santos, J. M., Eriksen, R., Moy, A. D., Sierro, F. J., Flores, J. A.,
787   et al. Limited variability in the phytoplankton *Emiliania huxleyi* since the pre-industrial
788   era in the Subantarctic Southern Ocean. Anthropocene, 31, 100254,
789   https://doi.org/10.1016/j.ancene.2020.100254, 2020b.

790   Rigual-Hernández, A. S., Trull, T. W., Nodder, S. D., Flores, J. A., Bostock, H., Abrantes, F., Eriksen,
791   R.S., Sierro, F. J., Davies, D. M., Ballegeer, A.-M., Fuertes, M. A., and Northcote, L. C.
792   Coccolithophore biodiversity controls carbonate export in the Southern Ocean,
793   Biogeosciences, 17, 245–263, https://doi.org/10.5194/bg-17-245-2020, 2020a.

794   Roth, P. H., and Berger, W. H. Distribution and dissolution of coccoliths in the South and Central
795   Pacific. Sliter, W. V., Be,´ A. W. H., Berger, W. H. (Eds.), Dissolution of Deep-Sea
796   Carbonates, Cushman Foundation Foraminiferal Research, Spec. Publ., N. 13, pp. 87-
797   113, 1975.

798   Roth, P. H., and Coulbourn, W. T. Floral and solution patterns of coccoliths in surface sediments
799   of the North Pacific. Mar. Micropaleontol., 7(1), 1-52, https://doi.org/10.1016/0377-
800   8398(82)90014-7, 1982.

801   Sarmiento, J. L., Gruber, N. Ocean Biogeochemical dynamics. Princeton, NJ, Woodstock:
802   Princeton University Press. 528 pp, 2006.

803   Schlitzer, R. Ocean data View. Available at:<htt://odv.awi.de>, 2019.

804   Stoll, H. M., Ziveri, P. Separation of monospecific and restricted coccolith assemblages from
805   sediments using differential settling velocity, Mar. Micropaleontol., 46(1–2), 209-221,
806   https://doi.org/10.1016/S0377-8398(02)00040-3, 2002.

807 Su, X., Liu, C., and Beaufort, L. Late Quaternary coccolith weight variations in the northern South

808   China Sea and their environmental controls, Mar. Micropaleontol., 154, 101798,

809   https://doi.org/10.1016/j.marmicro.2019.101798, 2020.

810 Subhas, A. V., Dong, S., Naviaux, J. D., Rollins, N. E., Ziveri, P., Gray, W., et al. Shallow calcium

811   carbonate cycling in the North Pacific Ocean, Global Biogeochem. Cy., 36(5), 1–22,

812   https://doi.org/10.1029/2022GB007388, 2022.

813 Sulpis, O., Boudreau, B. P., Mucci, A., Jenkins, C., Trossman, D. S., Arbic, B. K., and Key, R. M.

814   Current $CaCO_3$ dissolution at the seafloor caused by anthropogenic CO_2, P. Natl. Acad.

815   Sci. USA, 115(46), 11700–11705, https://doi.org/10.1073/pnas.1804250115, 2018.

816 Sulpis, O., Jeansson E., Dinauer A., Lauvset, S. K., and Middelburg, J. J. Calcium carbonate

817   dissolution patterns in the ocean, Nat. Geosci., 14(6), 423–428,

818   http://dx.doi.org/10.1038/s41561-021-00743-y, 2021.

819 Thunell, R. C., Qingmin, M., Calvert, S. E., and Pedersen, T. F. Glacial-Holocene biogenic

820   sedimentation patterns in the South China Sea: Productivity variations and surface

821   water pCO_2, Paleoceanography, 7(2), 143–162, https://doi.org/10.1029/92PA00278,

822   1992.

823 Tian, J., Huang, E., and Pak, D. K. East Asian winter monsoon variability over the last glacial cycle:

824   Insights from a latitudinal sea-surface temperature gradient across the South China Sea,

825   Palaeogeogr. Palaeocl., 292(1–2), 319–324,

826   https://doi.org/10.1016/j.palaeo.2010.04.005, 2010.

827 USGCRP. Climate Science Special Report: Fourth National Climate Assessment, Volume I

828   [Wuebbles, D. J., Fahey, D. W., Hibbard, K. A., Dokken, D. J., Stewart, B. C., and Maycock,

829   T. K. (eds.)]. U.S. Global Change Research Program, Washington, DC, USA, 470 pp., 2017.

830 Vollmar, N. M., Baumann, K. H., Saavedra-Pellitero, M., and Hernández-Almeida, I. Distribution

831   of coccoliths in surface sediments across the Drake Passage and calcification of *Emiliania*

832   *huxleyi* morphotypes, Biogeosciences, 19(3), 585–612, https://doi.org/10.5194/bg-19-

833   585-2022, 2022.

834 Wan, S., and Jian, Z. Deep water exchanges between the South China Sea and the Pacific since

835   the last glacial period, Paleoceanography, 29(12), 1162–1178,

836   https://doi.org/10.1002/2013PA002578, 2014.

837 Wan, S., Jian, Z., and Dang, H. Deep Hhydrography of the South China Sea and deep water

838   circulation in the Pacific since the Last Glacial Maximum, Geochem., Geophy., Geosy.,

839   19(5), 1447–1463, https://doi.org/10.1029/2017GC007377, 2018.

840   Wan, S., Jian, Z., Gong, X., Dang, H., Wu, J., and Qiao, P. Deep water [CO_3^{2-}] and circulation in
841   the South China Sea over the last glacial cycle, Quat. Sci. Rev., 243, 106499,
842   https://doi.org/10.1016/j.quascirev.2020.106499, 2020.

843   Wang, N., Huang, B.-Q., and Li, H. Deep-water carbonate dissolution in the northern South China
844   Sea during Marine Isotope Stage 3, J. Palaeogeogr., 5(1), 100–107,
845   https://doi.org/10.1016/j.jop.2015.11.004, 2016.

846   Wang, P., Li, Q., and Dai, M. The South China Sea Deep: Introduction, Deep-Sea Res. Pt. II: Top.
847   Stud. Oceanogr, 122, 1-5, https://doi.org/10.1016/j.dsr2.2015.11.004, 2015.

848   Wang, P., Wang, L., Bian, Y., and Jian, Z. Late Quaternary paleoceanography of the South China
849   Sea: surface circulation and carbonate cycles, Mar. Geol., 127(1–4), 145–165,
850   https://doi.org/10.1016/0025-3227(95)00008-M, 1995.

851   Wang, P. X., and Li, Q. Y. The South China Sea: Paleoceanography and Sedimentology. Springer,
852   Berlin, Heidelberg, New York, p. 506, 2009.

853   Young, J. R., and Ziveri, P. Calculation of coccolith volume and its use in calibration of carbonate
854   flux estimates, Deep-Sea Res. Pt. II: Top. Stud. Oceanogr., 47(9–11), 1679–1700,
855   https://doi.org/10.1016/S0967-0645(00)00003-5, 2000.

856   Yu, J., and Elderfield, H. Benthic foraminiferal B/Ca ratios reflect deep water carbonate
857   saturation state, Earth Planet. Sci. Lett., 258(1–2), 73–86,
858   https://doi.org/10.1016/j.epsl.2007.03.025, 2007.

859   Yu, J., Menviel, L., Jin, Z. D., Thornalley, D. J. R., S. Barker, S., Marino, G., et al. Sequestration of
860   carbon in the deep Atlantic during the last glaciation, Nat. Geosci., 9, 319-324,
861   https://doi.org/10.1038/ngeo2657, 2016.

862   Zachos, J. C., Röhl, U., Schellenberg, S. A., Sluijs, A., Hodell, D. A., Kelly, D. C., et al. Paleoclimate:
863   Rapid acidification of the ocean during the Paleocene-Eocene thermal maximum,
864   Science, 308(5728), 1611–1615, https://doi.org/10.1126/science.1109004, 2005.

865   Zhang, H., Liu, C., Jin, X., Shi, J., Zhao, S., and Jian, Z. Dynamics of primary productivity in the
866   northern South China Sea over the past 24,000 years, Geochem., Geophy., Geosy.,
867   17(12), 4878–4891, https://doi.org/10.1002/2016GC006602, 2016.

868